BOLETIN DE LA SOCIEDAD ESPAÑOLA DE
Cerámica y Vidrio
www.elsevier.es/bsecv

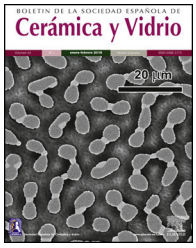

Effect of P_2O_5 and Al_2O_3 on crystallization, structure, microstructure and properties of $Li_2O–MgO–Al_2O_3–SiO_2–TiO_2–ZrO_2$ glass ceramics

Khalissa Ariane[a], *Aitana Tamayo*[b,*], *Abdellah Chorfa*[a,c], *Fausto Rubio*[b], *Juan Rubio*[b]

[a] *Institute of Optics and Precision Mechanics, Ferhat Abbas University Setif 1, Setif, Algeria*
[b] *Instituto de Cerámica y Vidrio.CSIC. Madrid, Spain*
[c] *Laboratory of applied optics, IOMP, Ferhat Abbas University Setif 1, Setif, Algeria*

ARTICLE INFO

Article history:
Received 22 May 2020
Accepted 4 August 2020
Available online 25 August 2020

Keywords:
Glass-ceramics
Nucleation
Thermal properties
Spectroscopy

ABSTRACT

The structure, microstructure, thermal and mechanical properties of glasses and glass-ceramics in the LMAS (Li_2O, MgO, Al_2O_3, SiO_2) system and the effect of P_2O_5 and Al_2O_3 additives have been studied. The transition temperatures of both glasses and glass-ceramics increase with the P_2O_5 and Al_2O_3 concentration, but at high temperatures the melt viscosity decreases. The main crystalline phases formed are lithium aluminium silicate, enstatite and β-spodumene, being the growth of β-spodumene favoured by fluorine ions, P_2O_5 and the heat treatment temperature as well. Raman and FT-IR spectroscopies have shown the formation a silica-rich glass phase which acts as a matrix of the crystallites containing Al_2O_3 and P_2O_5 in its composition. The shape and aspect ratio of the crystallites depend on the Al_2O_3 concentration. For low Al_2O_3 concentration a variety of tubular, granular and plate-like crystals appear, while for high Al_2O_3 concentration the main shape of the crystals is spherical or globular. H_v, *E* and *CTE* properties are related to the crystalline phases formed during the crystallization treatment, and their variations are in accordance with the increase of the crystal aspect ratio. The *CTE* values of the GCs decrease as the P_2O_5 content increases up to 3%, while for the Al_2O_3 concentration of 16% the minimum CTE value is obtained. H_v and *E* values of the GCs are higher than those corresponding to their respective parent glasses. According to these values, these glasses and glass-ceramics are not appropriate for machining.

* *Corresponding author.*
E-mail address: aitanath@icv.csic.es (A. Tamayo).
https://doi.org/10.1016/j.bsecv.2020.08.004

Efecto del P_2O_5 yAl_2O_3 en la cristalización, estructura, microestructura y propiedades de vitrocerámicos del sistema Li_2O-MgO-Al_2O_3-SiO_2-TiO_2-ZrO_2

Palabras clave:
Vitrocerámicos
Nucleación
Propiedades térmicas
Espectroscopía

RESUMEN

En este trabajo se ha estudiado el efecto del contenido en P_2O_5 y Al_2O_3 en vidrios y vitrocerámicos del sistema LMAS (Li_2O, MgO, Al_2O_3, SiO_2) en su estructura, microestructura y propiedades térmicas y mecánicas. La adición de estos dos óxidos produce el aumento de las temperaturas de transición tanto de los vidrios como de los vitrocerámicos correspondientes, sin embargo, la viscosidad a alta temperatura decrece. Las fases cristalinas que se forman son fundamentalmente silicato de litio-aluminio, enstatita y β-espodumena, donde el crecimiento de β-espodumena está favorecido por la presencia de iones F, P_2O_5 así como por la temperatura de tratamiento. Las espectroscopias Raman y FTIR han permitido detectar la formación de una fase vítrea rica en sílice que actúa como matriz de los cristales que contienen Al_2O_3 y P_2O_5 en su composición. La microestructura cristalina depende de la concentración de y Al_2O_3 en los vidrios. Para bajas concentraciones de Al_2O_3 se originan cristales con formas tubulares o con formas mientras que para altas concentraciones de Al_2O_3 los cristales tienen forma esférica o globular fundamentalmente. Los valores de H_V, *E* y *CTE* están relacionados con las fases cristalinas formadas durante el tratamiento de cristalización, y sus variaciones están relacionados con el factor de forma de los cristales. Los valores de CTE de los vitrocerámicos disminuyen a medida que el contenido de P_2O_5 aumenta hasta un 3%, mientras que para la concentración de Al_2O_3 del 16% se obtiene el valor mínimo de CTE. Los valores Hv y E de los GC son más altos que los correspondientes a sus respectivos vidrios principales. Estos valores indican que estos materiales, tanto vidrios como vitrocerámicos, no son apropiados para ser mecanizados.

Introduction

Glass-ceramics (GCs) are polycrystalline solids formed through the controlled crystallization of glasses. Crystallization is accomplished by subjecting appropriate glasses to a carefully regulated heat treatment schedule resulting in the nucleation and growth of crystal phases within the glass [1,2]. GCs are particularly interesting in several applications, such as thermal, chemical and mechanical, since they offer great possibilities for manipulating their properties such as transparency, strength and coefficient of thermal expansion (CTE) by modifying the composition and the heat treatment schedules [3]. Among the different GC, the most successful systems from the commercial point of view are the Li_2O–Al_2O_3–SiO_2 (Lithium-aluminosilicate system, LAS), and the MgO–Al_2O_3–SiO_2 (Magnesium-aluminosilicate system, MAS). Over the past three decades, much attention has been paid to the crystal phases and properties of LAS system due to its excellent thermo-physical properties [4] whereas the MAS system is attractive because of its good mechanical properties [4,5]. The major development of this system is hindered due to the high cost and high melting temperature. The addition of MgO to the LAS system, thus forming a Li_2O–MgO–Al_2O_3–SiO_2 (LMAS) system, helps to decrease the crystallization temperature and reduces the cost of the batch material but it has been rarely studied [6].

Different nucleating agents are normally employed highlighting TiO_2, ZrO_2, F and P_2O_5 as the most frequently used to increase the crystalline phases in GC systems. The mixture of the nucleating agents TiO_2, ZrO_2 and F exerts a synergistic effect on the crystallization mechanism of spodumene-willemite-diopside glasses [7]. It is also known that additions of P_2O_5 to certain silicate glass compositions promote volume nucleation and GC formation and markedly increases the crystal nucleation rate [8]. Bao et al. [9] have reported that the addition of B_2O_3 or P_2O_5 could promote the phase separation of glass, increase the size of the spherical phase separation droplet and decrease the crystallization temperature. Furthermore, the presence of fluorine in the parent glass enhances phase separation, reduces the crystallization temperature, refines the microstructure and improves the physical and mechanical properties of the GCs [10]. The fluorine content variation has a significant influence on the crystallization kinetics as well as the crystal morphology [10]. In addition to that, small amounts of Al_2O_3 will reduce the immiscibility in alkali silicate systems [11].

According to Bao et al. [9] the main crystalline phase in a LMAS glass-ceramic prepared by the solid state method are β-quartz solid solution ($Li_2Al_2Si_3O_{10}$), lithium silicate (Li_2SiO_3) and forsterite (M2P-16ASiO_4). Li et al. [12] also reported that the addition of MgO facilitates the phase transformation from β-quartz to β-spodumene in the LAS system. However, despite the wide use of MgO, its role on the crystallization reactions of LAS is not well understood. Zhang et al. [13] reported that with the increase of MgO content in Li_2O–ZnO–Al_2O_3–SiO_2 glass-ceramics, the glass transition temperature is barely modified

whereas the crystallization temperature decreases in a great extent, a fact which may be related with the effect of M2P-16A^{+} ion on the glass structure. According to Shi et Hou [14], the increase of MgO content in CaO–MgO–Al_2O_3–SiO_2 (CMAS) glass-ceramics made the vibration frequency of infrared spectrum shift to the low frequency which increases the average length of Si—O—Si bonds and causes the transformation of the crystal phase from wollastonite to pyroxene.

The presence of the different crystalline phases in LAS and LMAS GC systems causes a wide variation in the thermal and mechanical properties of the obtained materials [15]. In this sense, GC with coefficient of thermal expansion (CTE) from negative to positive values (−3.78 to $18.3 \times 10^{-6}\,^{\circ}C^{-1}$) can be obtained [16,17]. Moreover, LMAS GC materials can present microhardness values ranging from 4.8 GPa to 8.5 GPa [18]) and elastic modulus (E) between 75 and 100 GPa [19].

Although these materials are reported since long, scarce studies have been carried to discern the structure of these GC materials and the effect of the different crystalline phases. Previously [2] we have studied the effect of P_2O_5 and Al_2O_3 on the crystallization of LMAS GC materials and we have obtained the corresponding kinetic parameters. It was reported that increased amounts of P_2O_5 or high Al_2O_3 concentrations improve the glass stability and increase the crystallization temperature. In the present work we study the sintering and crystallization processes of LMAS GC containing TiO_2, ZrO_2, F and P_2O_5 by means of X-ray diffraction (XRD), Raman and Infrared spectroscopies (FTIR) and their correlations with the microstructure, thermal and mechanical properties. We will compare the behavior of a glass containing a high Al_2O_3 content with the remainder glasses containing the nucleating agents.

Experimental

Preparation of glasses and glass ceramics

The glasses used in this study were prepared as described in a previous work [2]. Four glass batches (80 g) with SiO_2, Al_2O_3, $MgCO_3$ (98.5%), Li_2CO_3, cryolite (Na_3AlF_6), TiO_2, Na_2CO_3, $ZrSiO_4$ and P_2O_5 as raw materials were prepared. The function of fluorine and P_2O_5 is to serve as nucleation agents. The amount of fluorine was maintained practically constant whereas P_2O_5 was added in increased concentrations of 0, 1.0, 2.0 and 3.0 mol%. Additionally, in order to study the effect of the Al_2O_3, another glass composition now containing 16 mol% of Al_2O_3 and without F was also prepared. The nominal composition of the prepared glasses is given in Table 1. The chemical composition, as analyzed by elemental analysis was also given in the above mentioned work and we have also included here just for comparison purposes [2]. All the elements except Li were determined by XRF (XRF, Philips, Magic Pro, USA). Li content was determined by ICP-EOS. In the case of fluorine determination, a special curve for the quantitative analysis of F was also used.

Different batches of glass samples were well mixed and calcined in a platinum crucible at 900 °C for 2 h, then melted at 1600 °C and held from 2 to 3 h (air atmosphere) in an electric furnace. The melt was poured onto a preheated metal plate and allowed to cool down at ambient temperature. To ensure homogeneity, the poured glasses were ground and re-melted at the same conditions for two additional hours and immediately annealed at 575 °C (near to transition temperature), for 4 h. The glasses were then slowly cooled inside the furnace with the aim to eliminate thermal residual stresses.

For obtaining GC materials, the annealed glass blocks were cut into pieces of about 2 mm thickness with a cutting machine (Buehler-Beta Grinder/Polisher) and then they were polished gradually using silicon carbide abrasive paper and finally with a 3 μ diamond disk. The samples were cleaned with rinsed water and ultrasonic cleaning. The samples were heat treated at 650, 700, 750, 800 and 840 °C for 1 h to obtain the GC materials whose corresponding main crystallization peak determined by Differential Thermal Analysis (DTA) [2].

Characterization

Glass transition temperatures (T_g: $10^{12.3}$ Pa.s), dilatometric softening temperature (T_{DS}) and the thermal expansion coefficients (CTE) for both glasses and glass ceramics were measured in a dilatometer (Bahr Thermo Analyze DIL 801 L, Hüllhorst, Germany) in dry air at a heating rate of 5 °C/min in the range of 25–1000 °C. For CTE determinations, sample pieces of 5 mm × 5 mm × 10 mm were used with Al_2O_3 as reference material. The characteristic temperatures were determined by using a Hot Stage Microscopy instrument (HSM, EM201 Leica) equipped with a CCD camera. The temperatures corresponding to the characteristic viscosity points (T_{IS}: initial shrinkage – 10^9 Pa s; T_{ES}: end of shrinkage – $10^{7.2}$ Pa s; T_D: Deformation-softening – $10^{5.1}$ Pa s; T_S: sphere – $10^{4.4}$ Pa s; T_{HS}: half sphere – $10^{3.6}$ Pa s and T_F: flow – $10^{3.1}$ Pa s) were obtained from the photographs taken during the HSM experiment and following Scholze's definition [1].

The crystalline phases developed in heat treated samples were determined by X-ray diffraction (XRD, Brucker D8-Advance, Germany) using Cu K_α radiation ($\lambda = 0.154059$ nm) with 2θ range of 10–70°, a scanning rate of $2^{\circ}\,min^{-1}$ and a 2θ interval of 0.01°. The developed phases were identified by JCPDS numbers (ICDD-PDF database).

The infrared spectra were obtained by using a Fourier-Transform Infrared Spectrophotometer (FT-IR, Perkin-Elmer Spectrum X) in the range 4000–400 cm^{-1} and a resolution of 2 cm^{-1}. Sample powders were mixed with KBr and pressed to get a transparent pellet. 16 scans were used to obtain a sample spectrum and background was subtracted every time. Raman spectra were measured in a Renishaw (In-Via, UK) spectrometer with a laser source of 514 nm. Raman spectra were recorded in the 1500–200 cm^{-1} range and at least 10 scans were used for each spectrum.

The microstructure of the crystalline phases developed after heat treatment was examined by Field Emission Scanning Electron Microscopy (FE-SEM, Hitachi 4700-S) operating at 20 kV. Fractured surfaces were etched, with HF solution (3%) for 15 s in order to eliminate the glass phase and after drying they were gold coated.

The Vickers hardness, *Hv*, was measured using a nano-indentation instrument (UMT-2, Bruker, Germany). Polished surfaces of the glass and glass-ceramic samples were indented

Table 1 – Nominal and chemical compositions (as determined by XRF) of the prepared glasses. All the compositions are given in mol%.

	Nominal composition								
	Li_2O	MgO	Al_2O_3	SiO_2	F	Na_2O	TiO_2	ZrO_2	P_2O_5
0P-5AF	10	15	5	55	7	1	5	2	0
1P-5AF	9.9	14.85	4.95	54.45	6.93	0.99	4.95	1.98	1
3P-5AF	9.7	14.55	4.85	53.35	6.79	0.97	4.85	1.94	3
2P-16A	9.3	14	16	51.25	0	0.93	4.66	1.86	2

	Chemical composition									
	Li_2O	MgO	Al_2O_3	SiO_2	CaO	Na_2O	TiO_2	ZrO_2	P_2O_5	F
0P-5AF	10.95	15.16	5.32	58.21	0.34	1.51	5.40	2.20	0.00	0.86
1P-5AF	11.28	15.00	5.31	57.41	0.33	1.82	5.37	2.13	0.81	0.46
3P-5AF	11.91	14.71	5.20	55.42	0.34	1.52	5.15	2.07	3.12	0.51
2P-16A	9.28	13.40	16.32	50.56	0.30	1.39	4.79	1.98	1.87	0

with a load (P) of 500 mN for 15 s. In all cases at least 10 indentations were made in order to get an error of ±0.2 GPa. The equations used for Hv determination was

$$H_v = 1.5844p/d^2 \quad (1)$$

where d is the mean of the diagonal lengths of the indentation finger in mm. From the Hv (Eq. (1)) the value the machinability parameter m and the cutting energy μ_1 were calculated according to [20]:

$$m = 0.643 - 0.122H_v \quad (2)$$

$$\mu_1 = {H_v}^{2.25} \quad (3)$$

Elastic modulus was obtained from the unloading curve of the indentation displacement using the Oliver–Pharr method [21].

Results and discussion

Chemical composition

The nominal and chemical composition of the different glasses is given in Table 1. All of them did not presented any crystalline peaks in the XRD (as it will be shown later) indicating a vitreous structure. The chemical composition of these glasses can be also found in a previous work published by our group [2]. It was observed that the amount of fluorine incorporated into the glass structure is significantly lower than the nominal values and this amount is even lower at the highest amounts of the other nucleating agent, P_2O_5.

Thermal characterization of glasses: dilatometry and HSM

Fig. 1a shows the thermal expansion curves for the prepared glasses. In the low-temperature region, between 100 and 500 °C, all the curves show a linear behaviour from where the *CTE* has been calculated. Above 500 °C, it is observed a change in the slope of the curves part until they reached the maximum dL/L_0 which corresponds to the dilatometric softening point (T_{DS}). The T_g value is calculated from the intersection of the two linear parts with different slopes. The calculated T_g, T_{DS} and CTE values in the different glasses are collected in Table 2. In general, by maintaining the Al_2O_3 concentration constant, the addition of P_2O_5 to the glass composition leads to an increase in both T_g and T_{DS} temperatures and an increase in the CTE. However, when Al_2O_3 amount is increased, the opposite behaviour was observed, with an increase in the two characteristic temperatures and a decrease in *CTE*. In phosphate-bearing glasses, it is expected that a decrease of the polymerization degree of the glassy phase would produce a decrease in the T_g value and an increase of the CTE [22]. The observed increase in of both the T_g and CTE with the phosphate content has been already observed by some other authors in devitrified glasses and attributed this behaviour to a phase separation and the obtaining of a composite CTE [23]. In the absence of a phase separation, the most plausible explanation for the observed behaviour is the decrease of the bond strength further enhanced by the formation of CaF^+ structural units that provide a minor crosslinking degree in the glass network [23,24].

Fig. 1b presents the corresponding HSM curves for the prepared glasses. As it can be observed, several steps are revealed which correspond to the different thermal stages occurring during sample heating. The optical images of HSM (not shown here) allow determining the temperatures at where the different events take place. Table 2 collects the characteristic temperatures determined from the HSM curves. From HSM, we could determine that the start of the shrinkage corresponds to the beginning of the first step while its end corresponds to the end of the second step. The third step corresponds to softening and flowing processes. The presence of two steps during shrinkage is an indication of crystallization processes during heating. The presence of the crystalline phases was already observed in another work [2] and their occurrence reduces or avoids the shrinkage process until they are formed. The two shrinkage steps take place at the temperature range comprised between 600 °C and 1100 °C, whereas the DTA peaks only appear between 700 °C and 850 °C, *i.e.* after the first step of the HSM curves. We can observe in Table 2 that the addition of P_2O_5 or Al_2O_3 to the glass composition increases the shrinkage temperature while the end of shrinkage is only affected by the Al_2O_3 concentration. We also the give the $\Delta T_x = \Delta T_{IS} - \Delta T_{ES}$

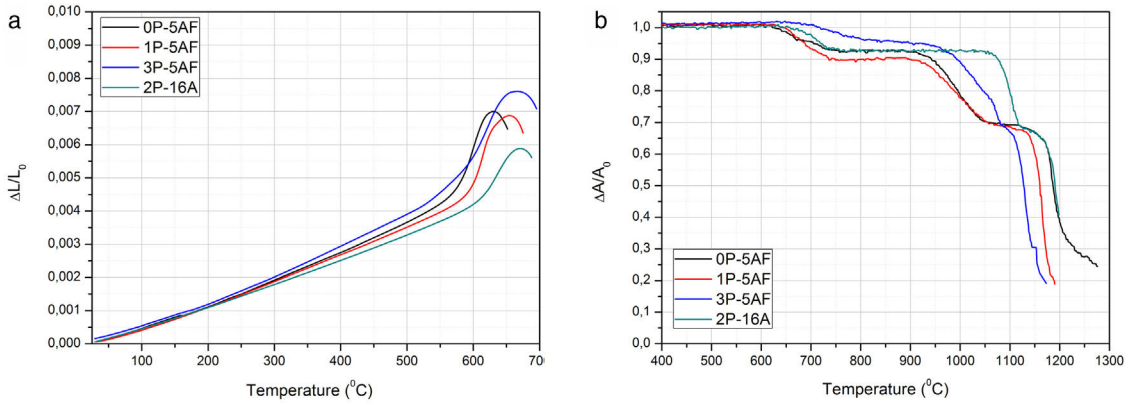

Fig. 1 – (a) Dilatometric curves and (b) HSM curves for the prepared glasses.

Table 2 – Characteristic temperatures and CTE for the as-prepared glasses. $\Delta T_x = T_{i1} - T_{e2}$.

	Dilatometric			HSM						
	CTE 10^{-6}100–500 °C	T_g (°C)	T_{DS} (°C)	1st step		2nd step		3rd step		
				Ti_1	Te_1	Ti_2	Te_2	ΔT_x	Ti_3	Te_3
0P-5AF	7.70	572	637	613	761	930	1097	484	1150	1230
1P-5AF	8.09	593	651	620	759	890	1059	439	1114	1188
3P-5AF	9.29	601	668	708	814	938	1088	380	1104	1166
2P-16A	7.35	578	672	640	743	1069	1133	493	1144	1196

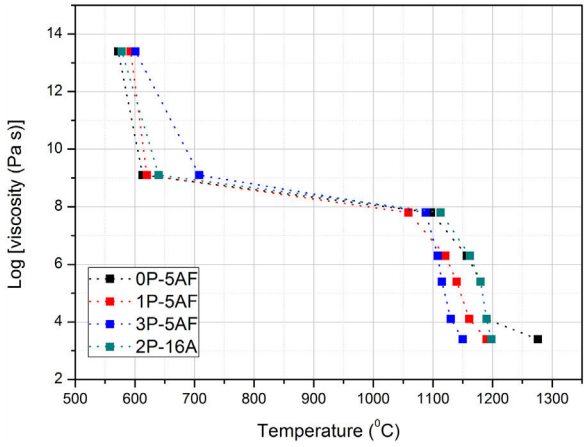

Fig. 2 – Viscosity of prepared glass samples (lines are only for guiding the eye).

values in Table 2 that correspond to the temperature differences between the start and the end of the shrinkage process *i.e.* between first and second steps of the HSM curves. There, it is now observed that the temperature range of the shrinkage process decreases with the P_2O_5 addition but increases with the Al_2O_3. This indicates that the formation of crystalline phases occurs in a low temperature interval as the P_2O_3 concentration increases.

From HSM and thermal expansion curves the characteristic temperatures can be determined. In accordance to the pioneer paper published by Scholze [25], each temperature can be assigned to a given fixed point of viscosity. Fig. 2 shows the evolution of the fixed points of viscosity for the prepared glasses. The glasses prepared by Toplis and Dingweel [26] with Na/(Na + Al) < 0.6 showed that the addition of P to a glass gives an increase in the viscosity until a concentration of P_2O_5 about 7% mol. As occurs in our materials, all the glasses containing equivalent amounts of Al_2O_3 present T_g values very close to each other but a small increase with the P_2O_5 concentration was determined. Besides, these glasses with similar Al_2O_3 concentration also show a temperature corresponding to the beginning of the shrinkage very close however, the glass labeled 2P-16A, that contains a high quantity of Al_2O_3, shifts the T_{IS} to the high temperature. The presence of Al_2O_3 thus slows down particle sintering.

From T_{IS1} to T_{ES2}, all the glasses present a wide temperature span (about 300 °C), a result that is directly related to the formation of crystalline phases [2]. In the high temperature range (above 1000 °C), it is observed that both the viscosity and the T_F fixed point (corresponding to a η value of $10^{3.4}$) decrease with the increase of P_2O_5 content (Fig. 2). Several authors have found similar results for Na/Al < 1 (see Table 1), and they have assigned this behavior to the ability of P_2O_5 for the formation of different structural units (monomers, dimers, extensive chains) with Na_2O and Al_2O_3 [26–28].

X-ray diffraction

In order to study the crystalline phases present in the 650–850 °C temperature range, several heat treatments for 1 h were also carried out. The crystallization temperatures, as determined by DTA were 755 °C for 0P-5AF, 760 °C for 1P-5AF, 837 °C for 3P-5AF and 764 °C for 2P-16A [2]. Fig. 3 shows the corresponding XRD patterns. Here is observed that all the as prepared glasses present a typical glass structure without

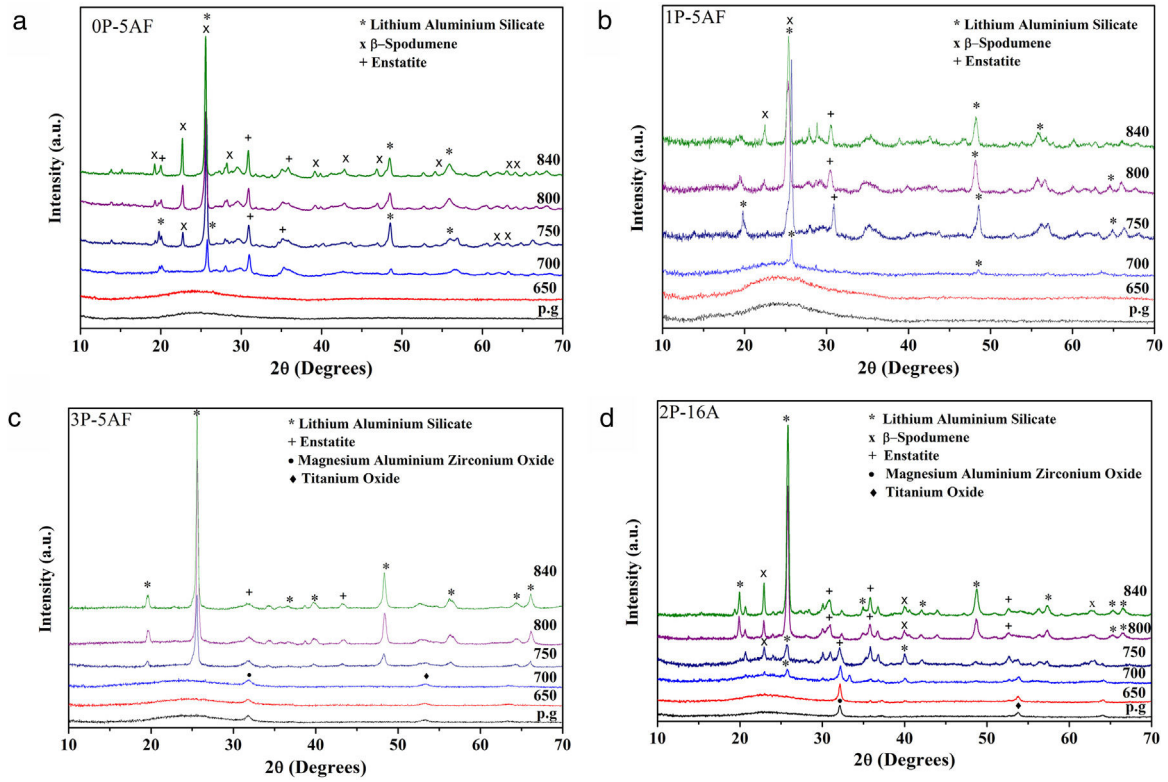

Fig. 3 – XRD patterns for 0P-5AF, 1P-5AF, 3P-5AF and 2P-16A glasses at 650, 700, 750, 800 and 840 °C.

diffractions peaks, although in the case of 3P-5AF and 2P-16A glasses, a small peak that does not increase with the heating treatment could be attributed to an impurity of a pseudo phase of magnesium aluminum zirconium oxide ($Mg_5Al_{2.4}Zr_{1.7}O_{12}$).

At 700 °C, all the glasses excepting the one labeled 2P-16A present incipient crystallization of hexagonal lithium aluminum silicate (LAS, code 00-040-0073). A similar LAS phase was reported by Xingzhong et al. [28] in glasses containing 18 Al_2O_3–68 SiO_2–4 Li_2O (mol %) with different nucleating agents at a heating at temperatures between 790 and of 830 °C and by Ananthanarayan et al. in glasses of 14 Al_2O_3–72 SiO_2–14 Li_2O (mol%) with 1.1 (mol %) P_2O_5 as nucleating agent at temperatures comprised between 600 to 925 °C [18]. At 750 °C the LAS phase is now observed in the 2P-16A glass and in the remainder glasses with an increase of the intensity of the crystallization peaks as the temperature increases. The main crystalline phases are β-spodumene ($LiAlSi_2O_6$, code 00-035-0797) and enstatite ($MgSiO_3$, code 00-022-0714). The formation of β-spodumene has been reported in numerous works in a wide range of compositions and for multiple nucleating agents. When TiO_2 is used, β-spodumene appears at temperatures as high as 820 °C [29] but the addition of P_2O_5 seems to delay the formation this phase, as occurs in our materials [30].

In the 2P-16A glass, which was prepared without F as nucleating agent, LAS is the main crystalline phase with a very small amount of β-spodumene, suggesting that F is necessary for the β-spodumene crystallization. Guo et al. demonstrated that little fluorine concentration in glasses improves the crystallization of β-spodumene decreasing the crystallization temperature about 110 °C with respect to the fluorine-free glass [31], being this crystallization even more promoted in the presence of both P_2O_5 and fluorine [32]. The above commented results imply that fluorine and P_2O_5 are nucleating agents that favor the formation of β-spodumene while P_2O_5 mainly favors the formation of the LAS phase.

Raman

The evolution of the glass structure after heat treatment between 650 °C and 850 °C for 1 h was further confirmed by Raman spectroscopy (Fig. 4). The spectra of the glasses 0P-5AF and 1P-5AF are typical of aluminum-silicate glasses with broad bands located close to 950 cm^{-1} and 800 cm^{-1} suggesting a quite disordered structure [33]. Silica glasses present the main bands are at 460, 800 and 1100 cm^{-1} due to the Si—O—Si bonds in Q^4 units [34]. Glass modifiers ions such as alkaline or alkaline-earth oxides induce the breakage of the Si—O—Si bonds leading to a decrease in the 460 cm^{-1} band and an increase of the 1100 cm^{-1} band [35]. The low intensity of the 200–500 cm^{-1} region indicates a large amount of broken Si—O^- units because of the alkaline ions used in the glass composition (Li^+ and Na^+). At the same time the incorporation of high field-strength cations (Al^{3+}, Zr^{4+}, Ti^{4+}) leads to a redshift of the 1100 cm^{-1} band indicating that these cations are forming part of a three-dimensional network in a four-fold coordination, probably acting as network formers [36,37]. The variation of the T—O—T angle (were T represents tetrahedrally coordinated network-forming cations such as Si, Al, Zr and/or Ti) in the glass is the responsible of the disorder and the corresponding broadening of the Raman bands. Moreover, the presence of Li^+

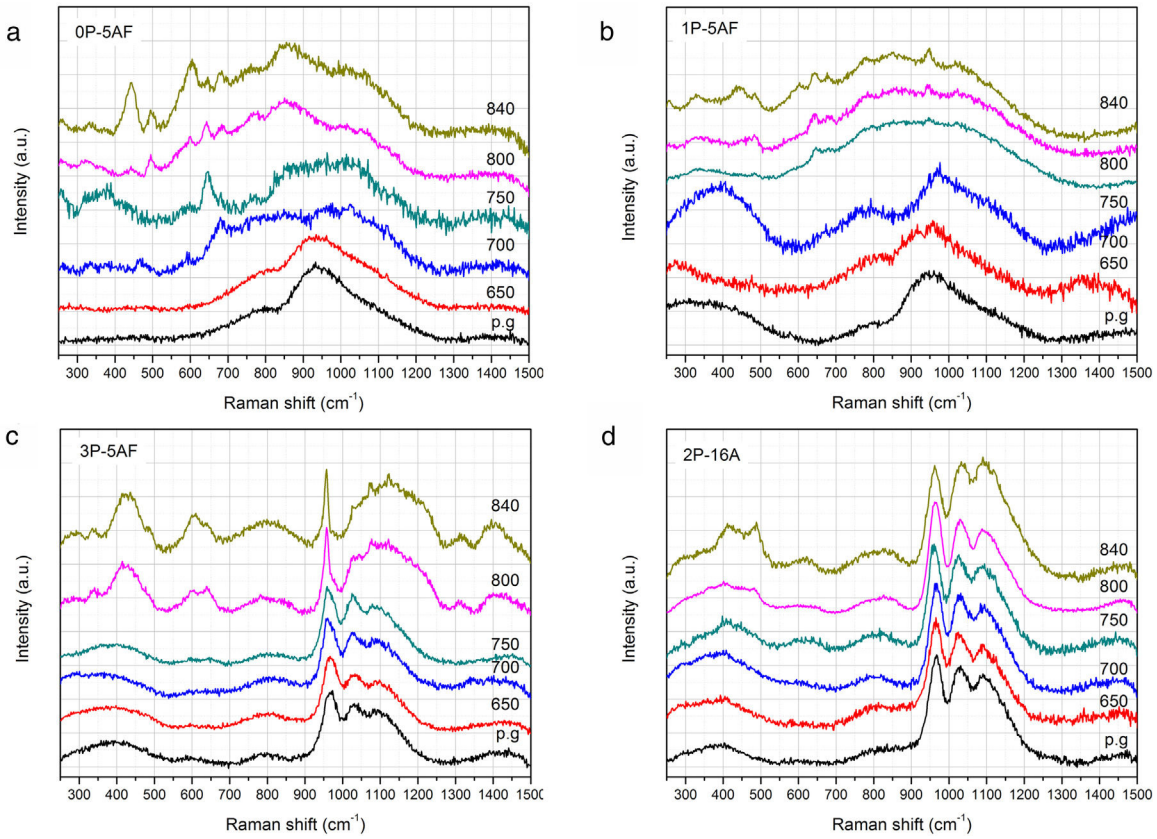

Fig. 4 – Raman spectra of 0P-5AF, 1P-5AF, 3P-5AF and 2P-16A glass-ceramics.

in the glasses causes an increase in the intensity of the bands in the 900–1200 cm^{-1} spectral region due to the formation of non-bridging oxygens (NBO) in the silicate network [34,35].

Similarly, as occurred in the XRD patterns, the Raman spectra of the 0P-5AF and 1P-5AF glasses heat treated at 650 °C are similar to those of the as-prepared ones, despite the treatment temperature is above T_g. By increasing the temperature to 700 °C the Raman bands becomes broader and some small bands also appear. Motion of Si and O atoms in Si—O—Si bonds is shown in the spectra at 800 cm^{-1} and the band tends to decrease with the depolymerization of the network i.e. with the formation of NBO (i.e. Si—O— bonds) [34]. In Fig. 4 we observe an increase of this band due to the formation of new Si—O—Si, Si—O—Al, Si—O—Zr or Si—O—Ti bonds in new crystalline phases. When silicate glasses are treated above their T_g, the spectral region 1000–1200 cm^{-1} increase in intensity and width forming an unique band as it is observed for the glasses treated at 800 and 850 °C [38]. The broadening of the above mentioned bands is clearer in 1P-5AF glass than in 0P-5AF, indicating that the addition of low P_2O_5 concentrations to the LMAS composition leads to a delay the formation of crystalline phases, as previously observed by XRD [30]. At 850 °C these glasses present well defined Raman bands located at 440, 500, 610, 650 and 685 and 950 cm^{-1} while those at 260, 340, 780 and 850 cm^{-1} are broad. All of these peaks must be assigned to the formation of different polymorphs of spodumene such as γ, β and α types [37] but their low intensities suggest that the obtained GC materials still present an important glass phase that is not totally crystallized. In the spectra, the band at 500 cm^{-1} is attributed to β-spodumene [37] and the bands at 650 and 680 cm^{-1} also can be assigned to pyroxene minerals such as enstatite ($MgSiO_3$) [33]. The broad band around 1360 cm^{-1} appearing in the 1P-5AF treated at 650 °C could be assigned to the P=O stretching vibration [39] and is the only band that could be attributed to the P—O bands because of its overlapping with Si—O—Si [40]. The asymmetric and symmetric stretching of P—O—P would appear at 620 and 1260 cm^{-1}, respectively whereas the symmetric stretching of a non-bridging oxygen at 1170 cm^{-1}. The characteristic symmetric stretching of the orthophosphate groups is normally found around 960 cm^{-1} [41]. The Li—O and Na—O vibrational modes are also difficult to detect because of the disorder at the Li and Na sites [42].

The incorporation of more than 4% of P_2O_5 in 3P-5AF produces important changes in the Raman spectra. Three broad and low intensity bands appear at 400, 600 and 800 cm^{-1} and another three high intensity and broad bands at 970, 1030 and 1100 cm^{-1} are attributed to P=O bonds [39]. In the low-frequency region the three bands be assigned to the presence of P_2O_5 in the glass structure by forming T—O—P bonds (were T = Si, Al, Zr or Ti) [39]. The presence of Si—O—Si and Si—O—M (M = Al, Mg, Zr and Ti) can influence the intensity of these bands [35,43]. Near 970 cm^{-1}, P_2O_5-bearing glasses such as Na_2O-P_2O_5-SiO_2 glasses present a Raman band assigned to the symmetric stretching vibration of P—O and P—O—Si tetrahedral bonds [44], while in orthophosphate and pyrophosphate

glasses this band is split in two at 957 cm^{-1} and 1010 cm^{-1} [45]. Zirconium phosphates [46] and aluminous glasses [47] also present the split band but it tends to convert to a single band the P_2O_5 concentration increases indicating that at this Raman shift it can be present the P atoms in different environments (Si, Al, Zr, Ti). Upon heat treatment, XRD diffractograms (Fig. 3) showed small crystallization peaks at 750 °C. Raman spectroscopy does not detect any structural change suggesting that the samples contain a high quantity of glass phase. By increasing the temperature to 800 and 840 °C, the 3P-5AF GC present several bands at 300, 340, 430, 600 and 640 cm^{-1} previously assigned to different γ, β and α spodumene polymorphs [37] and enstatite [33]. The sharp peak at 957 cm^{-1} involves PO_4^{3-} ions and can be assigned to γ-Li_3PO_4 [48]. The broad band between 1000 and 1270 cm^{-1} indicates that a glass network has been formed as it occurred in the 0P-5AF and 1P-5AF glasses. In the 3P-5AF glass this band is not present because of the higher concentration of P_2O_5 [38].

The three main peaks at 970, 1030 and 1100 cm^{-1} are maintained in 2P-16A glass and involve the participation of Al^{3+} cations in the glass or glass-ceramic structures forming Si-O(Al) silicate tetrahedral [47]. Because of the relatively low concentration of P=O bonds, it is quite difficult to distinguish these structures on the tail at the right of the 1100 cm^{-1} band. Nevertheless, the 957 cm^{-1} band, which is also found in the Raman spectra of orthophosphate and pyrophosphate species is assigned to the vibration of nonbridging O (P^O) or orthophosphate tetrahedral [45].

FT-IR

The structure of the glass and glass-ceramic samples has been also studied by FTIR spectroscopy. Fig. 5 shows the normalized FTIR absorption spectra of the as-prepared and heat treated LMAS glasses. The stretching bands of SiO_4 and PO_4 tetrahedra [49] results in a broad and high intensity band whose maximum is shifts from 1022 to 1064 cm^{-1} as the P_2O_5 concentration increases from 0 to 3, respectively. By increasing the Al_2O_3 content, this band is presented at lower wavenumber (1018 cm^{-1}). The high molecular weight of Al_2O_3 respect to SiO_2 and the high field-strength of Al^{3+} origins this shift thus confirming that Al is bonded to Si through Si-O-Al bonds. The presence of Si—O—Zr and Si—O—Ti bonds which give IR symmetric stretching bands between 950–975 cm^{-1} and 930–950 cm^{-1}, and anti-symmetric stretching appear between 1050 and 1200 cm^{-1} respectively, may enhance the broadness and intensity of the band [50]. In this spectral region and, specifically between 850 and 1000 cm^{-1} also appear the vibration of the Si—O— bands, i.e. the NBO formed by the alkaline ions (Li^+ and Na^+) [51]. The Si—O and P—O stretching vibrations appear as a non-symmetric band which starts at about 660 cm^{-1} and presents a maximum at 790 cm^{-1} which is independent of the P_2O_5 amount but shifts to 725 cm^{-1} for the 2P-16A. In this later glass, the presence of Si—O—Al bonds leads to a decrease of this band, moreover, the shoulder close to 790 cm^{-1} suggest the coexistence of Si—O bonds. Near 470 cm^{-1}, all the glasses present the bending vibrations of O—Si—O and Si—O—Si bonds. The 3P-5AF glass also shows shoulder at 580 cm^{-1} due to the high concentration of P_2O_5 and assigned to O—P—O and P—O—Si bonds [40].

No significant changes were observed in the spectra of the glasses heat treated at 650 °C, however, after heating at temperatures beyond 700 °C several changes occur. The band centered around 1000 cm^{-1} presents now several peaks. At 1080 cm^{-1}, the 0P-5AF presents a maximum which shifts to 1090 cm^{-1} in 3P-5AF because of the symmetric stretching of Si—O—Si bonds. This band decreases in intensity when the Al_2O_3 amount increases. By increasing the temperature of the treatment, the peak appearing at about 1017 cm^{-1} shifts to lower wavenumber. This band is assigned to the formation of lithium aluminosilicates and β-spodumene [52]. It should be noticed also that this is the most intense band in the spectra of the 2P-16A glass ceramic. Close to 1210 cm^{-1} for the 0P-5AF and 1P-5AF glass ceramics and to 1220 cm^{-1} for the 3P-5AF GC a shoulder attributed to the anti-symmetric stretching of Si—O—Si bonds [35] indicates the release of some SiO_2 during the formation of β-spodumene. A shoulder located at 920, 930 and 960 cm^{-1} for the glasses containing 0, 1 and 3% of P_2O_5, respectively, and at 900 cm^{-1} for the glass with 16% Al_2O_3 tends to the disappearance as the temperature increases. On its side, a new band appear at 850 cm^{-1} for low P_2O_5 content and 880 cm^{-1} for high P_2O_5 content which is attributed to the presence of this oxide. These shoulders could be associated to AlO_6 octahedral with NBO as well to the formation of new Si—O—Zr and Si—O—Ti bonds because the SiO_2 release after β-spodumene crystallization.

Between 740 and 780 cm^{-1} it appears the Al-O covalent bond in AlO_4 tetrahedron in aluminosilicates [53]. This band increases in intensity with both the P_2O_5 and Al_2O_3 concentrations in the glass and behaves similarly as the one located at 1010 cm^{-1} indicating that both correspond to the same crystal phase. The peak at 680 cm^{-1} is associated to the one at 560 cm^{-1} and can also be assigned to the vibrations of silicon-oxygen rings in $Na(Si_2O_5)$ phases [54]. In addition, the presence of two new peaks at 506 cm^{-1} and 560 cm^{-1} at low P_2O_5 concentration and assigned to AlO_6 octahedral [55] indicates that the amount of this oxide influences the formation of crystalline phases such as lithium aluminosilicate or β-spodumene [30]. For P_2O_5 concentrations lower that 1% the formation of β-spodumene is favored, while for higher P_2O_5 concentrations the lithium aluminosilicate is the main crystalline phase formed as it was observed by XRD and Raman.

Microstructure development

Fig. 6 shows the SEM photographs of the polished and chemically etched surfaces of the 0P-5AF, 1P-5AF, 2P-16A and 3P-5AF glasses heated at 840 °C for 1 h. It is clearly observed that, when the Al_2O_3 is maintained constant in the composition, all the glasses presented the same microstructure independently of the P_2O_5 content. For the 0P-5AF, 1P-5AF and 3P-5AF the crystals present a wide variety of crystal shapes with tubular, granular and plate-like microstructures, while for the 1P-5AF5 the crystals are mainly globular or spherical-shaped crystals. The plate-like crystals of the GC with different P_2O_5 concentration are interlocked while the globular crystals are independent one to other.

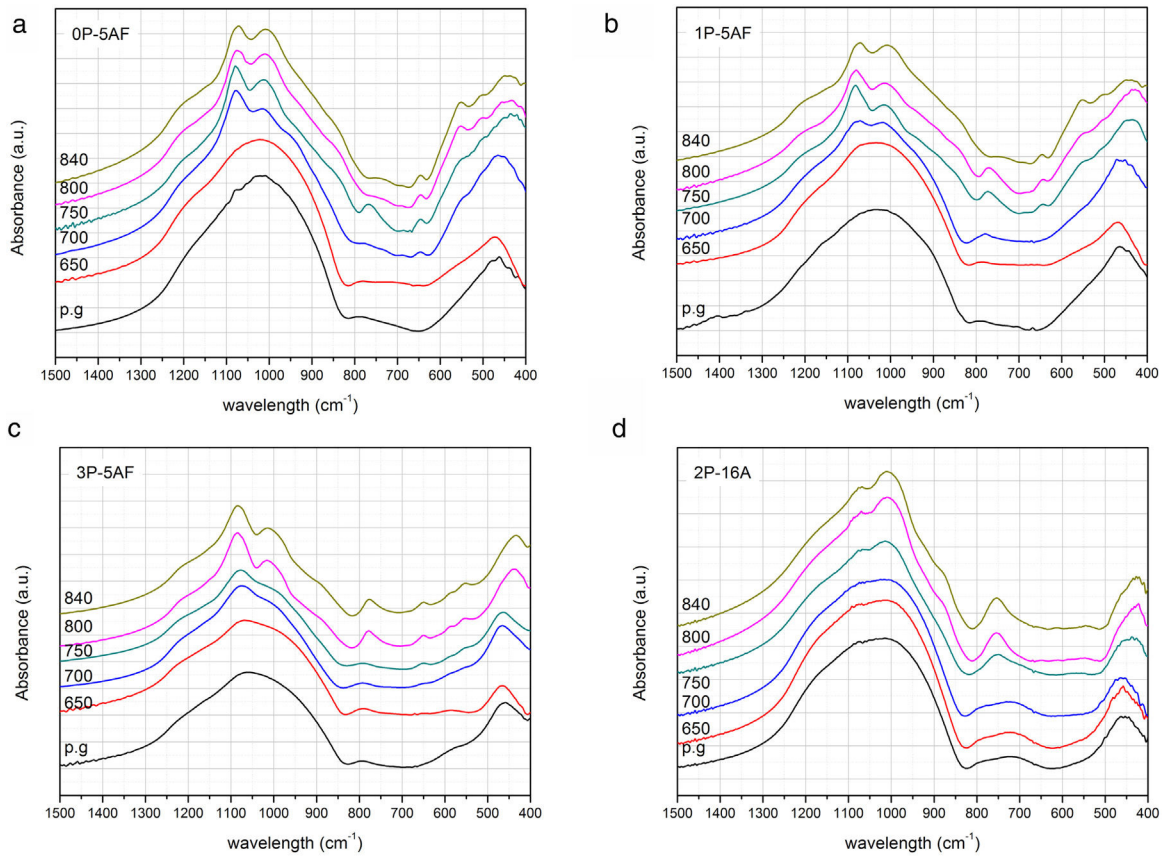

Fig. 5 – FT-IR spectra of (A) 0P-5AF, (B) 1P-5AF, (C) 2P-16A and (D) 3P-5AF glass-ceramic.

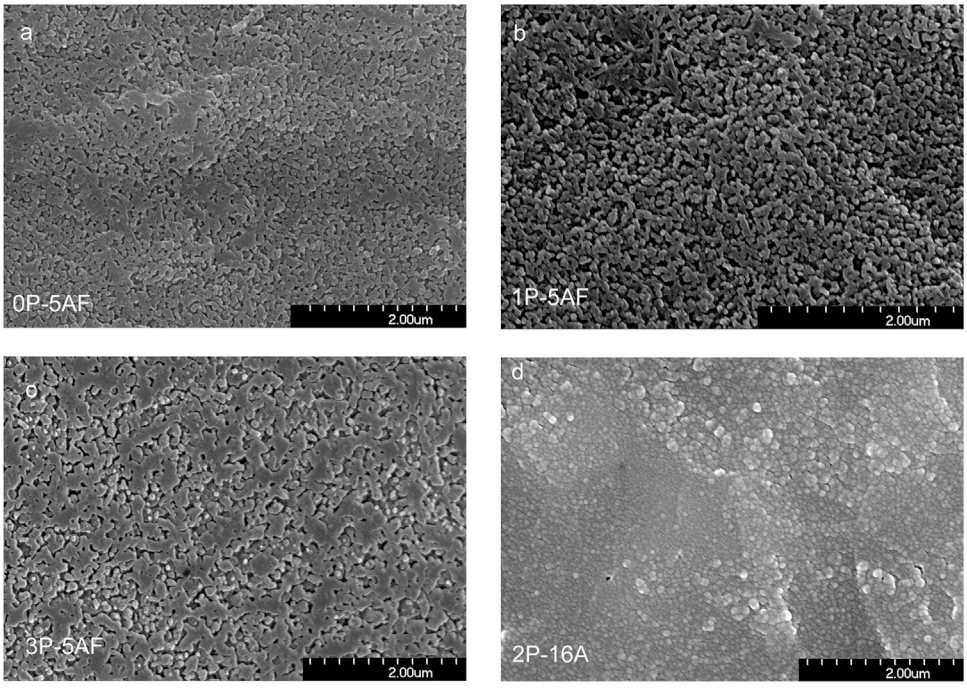

Fig. 6 – The SEM micrographs show the microstructure before and after heat treatment for 4 h at 755 °C, 764 °C, 764 °C and 837 °C for 0P-5AF, 1P-5AF, 2P-16A and 3P-5AF, respectively.

Table 3 – Microstructure (MCA, AR) and dilatometric (T_g, T_{DS}, CTE) properties of the LMAS GC materials.

	MCA (μm^2) 10^{-3}	AR	T_g [°C]	T_{DS} [°C]	CTE 10^{-6} [$°C^{-1}$]
0P-5AF	4.8	1.46	747	934	7.12
1P-5AF	2.8	1.43	846	858	5.89
3P-5AF	1.8	1.40	815	942	5.51
2P-16A	0.6	1.17	733	835	4.25

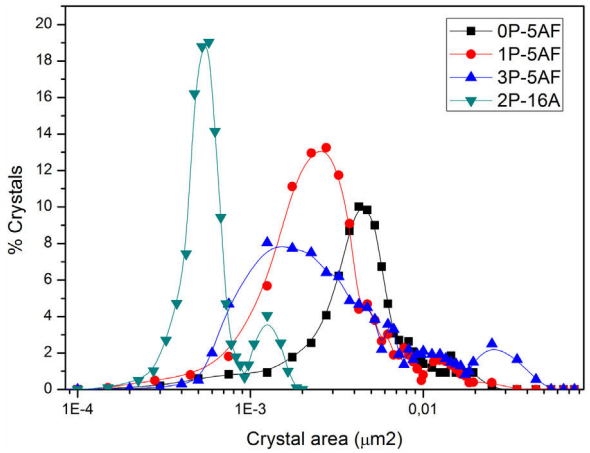

Fig. 7 – Area distributions of the crystals of the prepared GC materials .

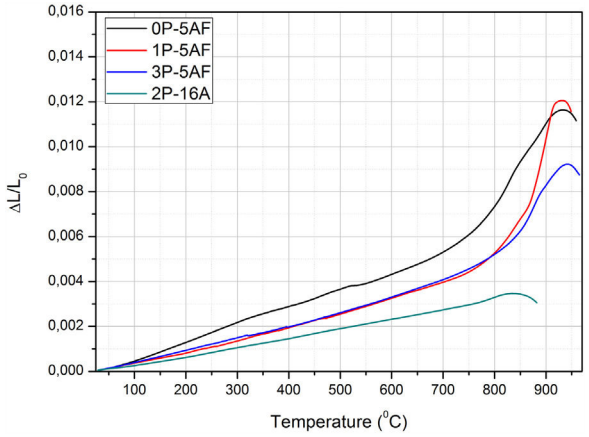

Fig. 8 – Thermal expansion curves of glass-ceramics.

Imaging analysis methods have been used to calculate the area and shape of the crystals appearing in Fig. 6. In Fig. 7 we have represented the distribution of the crystal area for the different GCs. Mean crystal area (*MCA*) and aspect ratio (*AR*) are resumed in Table 3. *AR* was determined by fitting the shape of the crystals to and ellipse and, the AR values are the ration between the two axes in the ellipse. Here it is observed that MCA and AR values tend to decrease with the P_2O_5 concentration in the glass and also, in the case of the AR value, the decrease is more pronounced in the case of a high Al_2O_3 content. By increasing either the P_2O_5 or Al_2O_3 the crystals tend to acquire a spherical form thus decreasing the area. In addition to that, as we observe in Fig. 7 the obtained LMAS materials present a bimodal crystal size distribution, with a maximum located near the MCA and another maximum at higher crystal area.

Glass-ceramic properties

CTE

After heat treatment of the glass materials at 860 °C, LMAS GC were obtained. The *CTE* curves shown in Fig. 8 are typical of glass-ceramic materials where crystalline phases are embedded in a glass phase and thus, we can observe that T_g and T_{DS} temperatures falls beyond the corresponding temperatures in their parent glasses (Fig. 1a). The calculated *CTE* values of the LMAS GC materials in the temperature range comprised between 100 and 500 °C and the above mentioned characteristic temperatures are collected in Table 3. The presence of several crystalline phases in the 0P-5AF GC induced the appearance of at least two regions with different slope in the low temperature range (the one used for CTE calculation). The change at about 350 °C can be assigned to a phase transition of α to β-cristobalite whereas at 525 °C is indicative of a combination of an α- to β-quartz transformation and γ- to β-lithium aluminosilicates [56] Although quartz has not been detected by XRD diffractograms, we might assume its presence in a very slow amount taking into consideration that the peak and shoulder at 1080 cm^{-1} and 1220 cm^{-1}, respectively, as well as the peak around 570 cm^{-1} in the FTIR spectra (Fig. 5) suggest the formation of a phase mainly composed by Si—O—Si bonds, i.e. a silica-rich residual glass phase or, probably, nano-crystals of quartz.

By comparing the values collected in Tables 2 and 3, we can observe that the addition of P_2O_5 reduces the thermal expansion of the GC in a great manner with respect to the parent glass, and this reduction is more noticed by increasing 16% Al_2O_3. T_g and T_{DS} increases in the LMAS GC. The observed results can be explained in terms of the crystalline phases detected in each LMAS GC material. Nevertheless, it must be taken into account that not only crystalline phases affect *CTE* but also the presence of the residual glass phase and its composition also influences in the structure of this residual glass [57].

Depending on the heat-treatment conditions, chemical composition, additives, type of crystalline phases present and their volume content in the GC, then *CTE* for lithium aluminosilicate glass-ceramics can be varied over a wide range [16,17,58–60]. The *CTE* values for the LMAS glass-ceramic materials obtained in this work and collected in Table 3 fits quite well with the bibliographic values. In general, the higher glass phase content in the GC material

Table 4 – Microhardness of parent glass and glass-ceramic samples.

	Hv [Gpa] (500 mN)		E [Gpa]		Machinability (m)		Cut energy m_1 (J mm^{-3})	
	G	GC	G	GC	G	GC	G	GC
0P-5AF	7.52	11.43	52.83	118.83	−0.27	−0.75	93.73	240.30
1P-5AF	8.40	11.46	75.95	118.03	−0.38	−0.75	120.04	241.58
3P-5AF	7.34	11.13	58.49	111.14	−0.25	−0.72	88.71	226.41
2P-16A	9.88	9.59	109.68	107.63	−0.56	−0.53	173.12	161.92

the higher *CTE* [59,60]. Besides, the type of crystals also influences in *CTE* values, thus authors which studied β-spodumene-virgilite GC, lithium silicate – lithium disilicate – quartz GC, lithium-magnesium-silicate-cristobalite GC and lithium-aluminosilicate – magnesium calcium silicate with ZrO_2 reported values comprised between .4–5.2 × 10^{-6} °C^{-1}, 9.95–14.68 × 10^{-6} °C^{-1}, 8.5 × 10^{-6} °C^{-1} and 2.2–2.7 × 10^{-6} °C^{-1}, respectively [59]. For a LAS GC the addition of P_2O_5 between 0 to 10% leads to an increase in CTE from 4.0 to 5.1 × 10^{-6} °C^{-1} [61]. The results of Table 3 show that the *CTE* of the LMAS GC decreases from 7.12 to 5.51 × 10^{-6} °C^{-1} a result that must indicate that the crystallinity of the LMAS GC increases with P_2O_5 addition and therefore the concentration of the residual glass phase decreases but by increasing the Al_2O_3 concentration *CTE* decreases [58]. By comparing the *CTE*s values with the corresponding *AR* values we obtained good correlation coefficients (r^2 = 0.85) and main crystal areas (r^2 = 0.97), showing the possibility to change the *CTE* of the GCs materials by changing the shape and size of the crystals.

Mechanical properties

The calculated values of *Hv*, *E*, *m* and μ_1 for the as-prepared glasses and their corresponding glass-ceramic materials are given in Table 4. Here, the presence of Si-O-Al bonds in the 2P-16A glass provides the highest *Hv* value [62] whereas no correlation with the P_2O_5 and the *Hv* value of the glasses has been found. In the case of the GC, the *Hv* values of the GC with the same 5% Al_2O_3 content are similar and in any case higher than the glass materials, probably due to the effect of annealing at temperatures lower than the T_g, which has been reported to cause an increase of the local strength of the GC intended for machining due to the elimination of uncontrollable distributions of the residual stress [63]. On contrary, annealing at temperatures above or around T_g may induce changes in the crystalline distribution, as deduced from the microplastic deformation observed in the mechanical testing [63]. The slight differences encountered in the prepared LMAS GC may outcome from their difference microstructures and the crystalline phases present (Fig. 6) [64]. Large crystal size and intertwined structures lead to high *Hv* values than globular microstructure of lower crystal size and independent of each other. Therefore, the 0P-5AF, 1P-5AF and 3P-5AF with high interlocking crystallinity lead to higher microhardness than the 2P-16A which presents non-interlocking crystallinity, i. e. the interlocking between crystals leads to a more rigid structure that corresponds to higher *Hv* values. Moreover, the *Hv* values are directly related to the shape or *AR* values of the crystals (cor.coef. 0.986), but the *Hv* increase is limited to a crystal size of 2.8 μm^2.

The same behavior as the one encountered in the *Hv* values is found in the case of *E* values. In general, for glass materials with a continuous microstructure, the elastic modulus is related to the chemical composition and their corresponding atomic bonding energy, packing density, network dimensionality and network topology (chains, rings, etc.) [65]. However, in the case of GC materials, the elastic modulus mostly depends on the microstructure and type of crystalline phases [64]. The globular structure of 2P-16A GC causes the decrease of the *E* value whereas the GC presenting a platelet-like crystallinity present higher *E* values. The delay in the formation of crystalline phases at the highest P_2O_5 concentration may be the responsible of the observed lower E value. In addition to that, *E* increases with *AR* but and *E* maximum value is obtained for crystal areas up to 2.8 μm^2, and higher crystal areas lead to a decrease in *E*.

The *m* and μ_1 parameters$_1$, calculated from *Hv* (Eqs. (2) and (3)) indicate that none of the prepared glasses and GC materials are appropriate for machining because of the negative m value and high μ_1 [34]. The *m* parameter is more negative in the GC materials than in the corresponding glasses and, at the same time, the μ_1 value is also higher, a result that indicates that these GC materials get worse machinability than their corresponding glasses.

Conclusions

Glasses in the LMAS (Li_2O, MgO, Al_2O_3, SiO_2) system with F, CaO, ZrO_2 and TiO_2 in their compositions have been prepared and crystallized to form glass-ceramic materials. The main conclusions are the following:

1. The characteristic T_g temperatures of both glasses and glass-ceramics increase with the P_2O_5 and Al_2O_3 concentrations. At high temperature the viscosity decreases with the Al_2O_3 concentration.
2. The formation of crystalline phases occurs between 600 and 900 °C, being the main phases β-spodumene, lithium aluminum silicate and a low concentration of enstatite. The P_2O_5 delays the formation of β-spodumene. F is necessary for the formation of β-spodumene and this crystalline phase is improved if both F- and P_2O_5 are present in the glass. β-spoduene tends to increase with heat treatment crystallization temperature.
3. From Raman and IR spectroscopies has been observed the presence of a glass phase which forms the matrix where the crystalline phases grow. In this glass phase the Al, Ti

and Zr cations probably acts as network formers while Li produces the formation of non-bridging oxygens. Si—O—Si, Si—O—Al, Si—O—Zr and Si—O—Ti bonds give different bands in the Raman spectra. Enstatite ($MgSiO_3$) bands can be also observed. P—O. O—P—O and Si—O—P bands are also observed mainly in those glasses with high P_2O_5 concentrations. The presence of β-spodumene and lithium aluminosilicate phases have been also observed by IR and Raman techniques and when these phases are formed a silica-rich glass phase is released and in it remains as a matrix where the crystals are embedded. The formation of these crystalline phases is favoured by the P_2O_5 addition.

4. For low Al_2O_3 concentration the microstructure presents a wide variety of crystal phases with tubular, granular and plate-like shapes, while for high Al_2O_3 concentration a globular or spherical-like microstructure appears. The mean crystal area and aspect ratio decrease with both the P_2O_5 and Al_2O_3 concentrations.
5. The silica rich glass phase is mainly constituted by SiO_2, Al_2O_3 and P_2O_5. This leads to an increase in the transformation and softening dilatometric temperatures of the GC materials.
6. The *CTE* values are in accordance with the crystalline phases present in the GCs but its variation is mainly due to the microstructure of the GCs. Because these GCs present the same type of crystal phases, the *CTEs* increase with both the decrease of the MCA and AR.
7. Mechanical properties are also correlated with the crystalline microstructures presented in the GCs, but it is observed that while *Hv* increases with AR of the crystals but only increase up to 2.8 mm^2 of crystal area, higher values of crystal areas do not influence in H_V. The same occurs for *E* property.
8. The machinability parameter and cutting energy indicate that all of these glasses and GCs are not appropriate for machining and that both Al_2O_3 and P_2O_5 lead to a decrease in their machinability.

Acknowledgements

The present work was supported by the Algerian Ministry of Higher Education and Scientific Research (Algerian program P.N.E 2016-2017 scholarship fund) and with the collaboration of the Institute of Ceramic and Glass ICV-CSIC, Madrid, Spain supported by project MAT2016-78700-R financed by Spanish Research Agency and European Regional Development Fund (AEI/FEDER, UE). The authors are also grateful to C. Díaz Dorado for her help with FE-SEM images.

REFERENCES

[1] P.W. McMillan, Glass-ceramics, Academic Press, London, 1964.
[2] K. Ariane, A. Tamayo, A. Chorfa, F. Rubio, J. Rubio, Kinetic study on the effect of adding P_2O_5 to the LMAS glass-ceramic, Boletín de la Sociedad Española de Cerámica y Vidrio (2019).
[3] L.R. Pinckney, G.H. Beall, Microstructural evolution in some silicate glass-ceramics: a review, J. Am. Ceram. Soc. 91 (2008) 773–779.
[4] G. Beall, Design and properties of glass-ceramics, Annu. Rev. Mater. Sci. 22 (1992) 91–119.
[5] L. Han, J. Song, C. Lin, J. Liu, T. Liu, Q. Zhang, Z. Luo, A. Lu, Crystallization, structure and properties of $MgO–Al_2O_3–SiO_2$ highly crystalline transparent glass-ceramics nucleated by multiple nucleating agents, J. Eur. Ceram. Soc. 38 (2018) 4533–4542.
[6] O.A. Al-Harbi, Effect of different nucleation catalysts on the crystallization of $Li_2O–ZnO–MgO–Al_2O_3–SiO_2$ glasses, Ceram. Int. 35 (2009) 1121–1128.
[7] A. El-Shennawi, A. Omar, A. Morsy, The role of titania and titania mixtures in the nucleation and crystallization of spodumene-willemite-diopside glasses, Thermochim. Acta 58 (1982) 125–153.
[8] Y. Iqbal, W. Lee, D. Holland, P. James, Crystal nucleation in P_2O_5-doped lithium disilicate glasses, J. Mater. Sci. 34 (1999) 4399–4411.
[9] Z.H. Bao, L.F. Miao, W.H. Jiang, J.M. Liu, J. Liang, T. Chen, Effect of B_2O_3 and P_2O_5 addition on the phase separation and crystallization of $Li_2O–MgO–Al_2O_3–SiO_2$ glass-ceramics, materials science forum, Trans. Tech. Publ. (2016) 243–248.
[10] L. Radonjić, L. Nikolić, The effect of fluorine source and concentration on the crystallization of machinable glass-ceramics, J. Eur. Ceram. Soc. 7 (1991) 11–16.
[11] M. Fairweather, J. Topping, M. Murthy, Effect of Al_2O_3 on a complex $Li_2O–ZnO–SiO_2$ glass-ceramic, J. Am. Ceram. Soc. 58 (1975) 260.
[12] Y. Li, B. Xu, J. Cao, L. Liang, K. Liang, Effect of MgO addition on crystallization and microstructure of $Li_2O–Al_2O_3–SiO_2–Ta_2O_5$ glass-ceramics, Phys. Chem. Glasses-Eur. J. Glass Sci. Technol. B 51 (2010) 173–178.
[13] Y. Zhang, Z. Luo, T. Liu, X. Hao, Z. Li, A. Lu, MgO-doping in the $Li_2O–ZnO–Al_2O_3–SiO_2$ glass-ceramics for better sealing with steel, J. Non-Crystal. Solids 405 (2014) 170–175.
[14] H.N. Shi, X.H. Hou, Effect of MgO on the crystallization behavior and properties of glass-ceramics, Trans. Indian Ceram. Soc. 77 (2018) 118–122.
[15] X. Hao, X. Hu, Z. Luo, T. Liu, Z. Li, T. Wu, A. Lu, Y. Tang, Preparation and properties of transparent cordierite-based glass-ceramics with high crystallinity, Ceram. Int. 41 (2015) 14130–14136.
[16] O. García-Moreno, A. Fernández, S. Khainakov, R. Torrecillas, Negative thermal expansion of lithium aluminosilicate ceramics at cryogenic temperatures, Scr. Mater. 63 (2010) 170–173.
[17] M. Bengisu, R.K. Brow, Effect of long-term heating and thermal cycling on thermal expansion, phase distribution, and microhardness of lithium aluminosilicate glass-ceramics, J. Non-Crystal. Solids 331 (2003) 137–144.
[18] A. Ananthanarayanan, G. Kothiyal, L. Montagne, B. Revel, MAS-NMR studies of lithium aluminum silicate (LAS) glasses and glass–ceramics having different Li_2O/Al_2O_3 ratio, J. Solid State Chem. 183 (2010) 120–127.
[19] W. Lien, H.W. Roberts, J.A. Platt, K.S. Vandewalle, T.J. Hill, T.M.G. Chu, Microstructural evolution and physical behavior of a lithium disilicate glass–ceramic, Dental Mater. 31 (2015) 928–940.
[20] D. Baik, K. No, J. Chun, Y. Yoon, H. Cho, A comparative evaluation method of machinability for mica-based glass-ceramics, J. Mater. Sci. 30 (1995) 1801–1806.
[21] W.C. Oliver, G.M. Pharr, An improved technique for determining hardness and elastic modulus using load and displacement sensing indentation experiments, J. Mater. Res. 7 (1992) 1564–1583.
[22] H. Grussaute, L. Montagne, G. Palavit, J.L. Bernard, Phosphate speciation in $Na_2O–CaO–P_2O_5–SiO_2$ and $Na_2O–TiO_2–P_2O_5–SiO_2$ glasses, J. Non-Crystal. Solids (2000) 312–317, 263-264.

[23] M.D. O'Donnell, S.J. Watts, R.V. Law, R.G. Hill, Effect of P_2O_5 content in two series of soda lime phosphosilicate glasses on structure and properties – Part II: Physical properties, J. Non-Crystal. Solids 354 (2008) 3561–3566.
[24] D.S. Brauer, M.N. Anjum, M. Mneimne, R.M. Wilson, H. Doweidar, R.G. Hill, Fluoride-containing bioactive glass-ceramics, J. Non-Crystal. Solids 358 (2012) 1438–1442.
[25] H. Scholze, The influence of viscosity and surface tension on hot-stage microscope measurement of glasses, Glastech. Ber. 39 (1962) 63–68.
[26] M. Toplis, D. Dingwell, The variable influence of P_2O_5 on the viscosity of melts of differing alkali/aluminium ratio: implications for the structural role of phosphorus in silicate melts, Geochim. Cosmochim. Acta 60 (1996) 4107–4121.
[27] M. Bengisu, R.K. Brow, A. Wittenauer, Glasses and glass-ceramics in the $SrO–TiO_2–Al_2O_3–SiO_2–B_2O_3$ system and the effect of P_2O_5 additions, J. Mater. Sci. 43 (2008) 3531–3538.
[28] G. Xingzhong, Z. Lingjie, Y. Hui, Effects of Li replacement on the nucleation, crystallization and microstructure of $Li_2O–Al_2O_3–SiO_2$ glass, J. Non-Crystal. Solids 354 (2008) 4031–4036.
[29] Y.-M. Sung, S.A. Dunn, J.A. Koutsky, The effect of boria and titania addition on the crystallization and sintering behavior of $Li_2O–Al_2O_3–4SiO_2$ glass, J. Eur. Ceram. Soc. 14 (1994) 455–462.
[30] J.J. Shyu, H.H. Lee, Sintering, crystallization, and properties of B_2O_3/P_2O_5-doped $Li_2O–Al_2O_3–4SiO_2$ glass-ceramics, J. Am. Ceram. Soc. 78 (1995) 2161–2167.
[31] X. Guo, H. Yang, M. Cao, Nucleation and crystallization behavior of $Li_2O–Al_2O_3–SiO_2$ system glass–ceramic containing little fluorine and no-fluorine, J. Non-Crystal. Solids 351 (2005) 2133–2137.
[32] X. Guo, X. Cai, J. Song, G. Yang, H. Yang, Crystallization and microstructure of $CaO–MgO–Al_2O_3–SiO_2$ glass–ceramics containing complex nucleation agents, J. Non-Crystal. Solids 405 (2014) 63–67.
[33] O. Dymshits, I. Alekseeva, A. Zhilin, M.Y. Tsenter, P. Loiko, N. Skoptsov, A. Malyarevich, K. Yumashev, X. Mateos, A. Baranov, Structural characteristics and spectral properties of novel transparent lithium aluminosilicate glass-ceramics containing (Er, Yb) NbO_4 nanocrystals, J. Lumin. 160 (2015) 337–345.
[34] C. Mulder, Defect structures in silica glass, J. Non-Crystal. Solids 95 (1987) 303–310.
[35] S. Perez-Villar, A. Tamayo, M.A. Mazo, F. Rubio, J. Rubio, Application of the Raman and IR/ATR spectroscopies to the study of the glasses upon grinding, Boletin De La Sociedad Espanola De Ceramica Y Vidrio 47 (2008) 89–94.
[36] Y. Li, K. Liang, J. Cao, B. Xu, Spectroscopy and structural state of V4+ions in lithium aluminosilicate glass and glass–ceramics, J. Non-Crystal. Solids 356 (2010) 502–508.
[37] S.K. Sharma, B. Simons, Raman study of crystalline polymorphs and glasses of spodumene composition quenched from various pressures, Am. Miner. 66 (1981) 118–126.
[38] P.F. McMillan, B.T. Poe, P.H. Gillet, B. Reynard, A study of SiO_2 glass and supercooled liquid to 1950K via high-temperature Raman spectroscopy, Geochim. Cosmochim. Acta 58 (1994) 3653–3664.
[39] C. Haiyan, H. Guosong, M. Hanfen, G. Fuxi, Structure and Raman spectra of glasses containing several glass-forming oxides and no glass-modifying oxide, J. Non-Crystal. Solids 80 (1986) 152–159.
[40] H. Aguiar, J. Serra, P. González, B. León, Structural study of sol–gel silicate glasses by IR and Raman spectroscopies, J. Non-Crystal. Solids 355 (2009) 475–480.
[41] A.K. Yadav, P. Singh, A review of the structures of oxide glasses by Raman spectroscopy, RSC Adv. 5 (2015) 67583–67609.
[42] Y. Hase, I. Yoshida, Low frequency bands of Li_2CO_3 crystal, Spectrochim. Acta A: Mol. Spectrosc. 35 (1979) 379.
[43] P. McMillan, Structural studies of silicate glasses and melts—applications and limitations of Raman spectroscopy, Am. Mineral. 69 (1984) 622–644.
[44] C. Nelson, D.R. Tallant, Raman studies of sodium silicate glasses with low phosphate contents, Phys. Chem. Glasses 25 (1984) 31–38.
[45] R. Dupree, D. Holland, M. Mortuza, The role of small amounts of P_2O_5 in the structure of alkali disilicate glasses, Phys. Chem. Glasses 29 (1988) 18–21.
[46] G.A. Mekhemer, Characterization of phosphated zirconia by XRD, Raman and IR spectroscopy, Colloids Surf. A: Physicochem. Eng. Aspects 141 (1998) 227–235.
[47] H. Gan, P.C. Hess, Phosphate speciation in potassium aluminosilicate glasses, Am. Mineral. 77 (1992) 495–506.
[48] L. Popović, B. Manoun, D. De Waal, M. Nieuwoudt, J. Comins, Raman spectroscopic study of phase transitions in Li_3PO_4, J. Raman Spectrosc. 34 (2003) 77–83.
[49] Y. Sun, Z. Zhang, L. Liu, X. Wang, FTIR, Raman and NMR investigation of $CaO–SiO_2–P_2O_5$ and $CaO–SiO_2–TiO_2–P_2O_5$ glasses, J. Non-Crystal. Solids 420 (2015) 26–33.
[50] Z. Congshen, H. Lison, G. Fuxi, J. Zhonghong, Low temperature synthesis of $ZrO_2–TiO_2–SiO_2$ glasses from Zr $(NO_3)_4·5H_2O$, Si $(OC_2H_5)_4$ and Ti $(OC_4H_9)_4$ by the sol-gel method, J. Non-Crystal. Solids 63 (1984) 105–115.
[51] F. Gan, G. Huang, S. Chen, Vibrational spectra of multicomponent inorganic glasses, J. Non-Crystal. Solids 52 (1982) 203–210.
[52] M. Chatterjee, M.K. Naskar, Sol–gel synthesis of lithium aluminum silicate powders: the effect of silica source, Ceram. Int. 32 (2006) 623–632.
[53] L. Han, J. Song, Q. Zhang, Z. Luo, A. Lu, Crystallization, structure and characterization of $MgO–Al_2O_3–SiO_2–P_2O_5$ transparent glass-ceramics with high crystallinity, J. Non-Crystal. Solids 481 (2018) 123–131.
[54] M. Sitarz, The structure of simple silicate glasses in the light of Middle Infrared spectroscopy studies, J. Non-Crystal. Solids 357 (2011) 1603–1608.
[55] B.N. Roy, Spectroscopic analysis of the structure of silicate glasses along the joint $xMAlO_2·(1–x)\ SiO_2$ (M = Li, Na, K, Rb, Cs), J. Am. Ceram. Soc. 70 (1987) 183–192.
[56] I. Donald, B. Metcalfe, A. Morris, Influence of transition metal oxide additions on the crystallization kinetics, microstructures and thermal expansion characteristics of a lithium zinc silicate glass, J. Mater. Sci. 27 (1992) 2979–2999.
[57] H. Darwish, S.N. Salama, S. Salman, Contribution of germanium dioxide to the thermal expansion characteristics of some borosilicate glasses and their corresponding glass-ceramics, Thermochim. Acta 374 (2001) 129–135.
[58] D. Tulyaganov, S. Agathopoulos, I. Kansal, P. Valerio, M. Ribeiro, J. Ferreira, Synthesis and properties of lithium disilicate glass-ceramics in the system $SiO_2–Al_2O_3–K_2O–Li_2O$, Ceram. Int. 35 (2009) 3013–3019.
[59] B. Li, S. Wang, Y. Fang, Effect of Cr_2O_3 addition on crystallization, microstructure and properties of $Li_2O–Al_2O_3–SiO_2$ glass-ceramics, J. Alloys Compd. 693 (2017) 9–15.
[60] O. García-Moreno, A. Borrell, B. Bittmann, A. Fernández, R. Torrecillas, Alumina reinforced eucryptite ceramics: very low thermal expansion material with improved mechanical properties, J. Eur. Ceram. Soc. 31 (2011) 1641–1648.

[61] Z. Xiao, J. Zhou, Y. Wang, M. Luo, Microstructure and properties of Li_2O–Al_2O_3–SiO_2–P_2O_5 glass-ceramics, Open Mater. Sci. J. (2011) 5.
[62] J.M. Fernandez-Navarro, El vidrio, 3rd ed., CSIC, Madrid, 2003, pp. 720.
[63] H. Fischer, M. Hemelik, R. Telle, R. Marx, Influence of annealing temperature on the strength of dental glass ceramic materials, Dental Mater. 21 (2005) 671–677.
[64] D.P. Mukherjee, A.R. Molla, S.K. Das, The influence of MgF2 content on the characteristic improvement of machinable glass ceramics, J. Non-Crystal. Solids 433 (2016) 51–59.
[65] D.L. Sidebottom, The fragility of alkali silicate glass melts: part of a universal topological pattern, J. Non-Crystal. Solids 516 (2019) 63–66.